XLVI CILAMCE
VITÓRIA - ES - BRAZIL - 2025
XLVI IBERO-LATIN AMERICAN CONGRESS ON COMPUTATIONAL METHODS IN ENGINEERING

Neural Network Application for Aerodynamic Force Estimation in Heavy Artillery Projectile Trajectories

AMARAL, L.G.[1], SOUSA, D. H. B[1], REZENDE, A. L. T.[1]

[1]*Seção de Engenharia Mecânica, Instituto Militar de Engenharia*
Praça Gen. Tibúrcio, 80 - Urca, 22290-270, Rio de Janeiro - RJ, Brasil
lucas.amaral@ime.eb.br, braz.daniel@ime.eb.br, arezende@ime.eb.br

Abstract. This work proposes the use of a neural network to estimate components of the aerodynamic forces acting on the trajectory of a 155 mm projectile. The approach aims to replace analytical expressions with a machine learning-based model, in order to compare the computational efficiency and flexibility of ballistic modeling techniques. The network was designed to estimate, based on the projectile's aerodynamic coefficients, the lift, drag, Magnus effect, rotational damping forces, and the projectile's angular adjustment. The dataset used for training was generated through the analysis of aerodynamic coefficients using the ballistic software PRODAS, considering different elevations, muzzle velocities, and atmospheric conditions. For validation, real firing data under various conditions were employed. The results show a mean squared error on the order of 3.10^{-3} and a correlation coefficient (R^2) above 0.9, indicating that the neural network is capable of adequately reproducing aerodynamic effects and presents itself as a viable alternative to traditional models.

Keywords: Neural Networks, Aerodynamic Coefficients, Heavy Artillery, External Ballistics.

1 Introduction

In recent decades, artificial intelligence (AI) has notably influenced engineering and defense. Neural networks (NNs), in particular, have proven effective in modeling complex systems, recognizing patterns, and supporting decisions under uncertainty. NNs have been applied to autonomous systems by Kebria [1], surveillance by Ullah [2], and aerodynamic coefficient estimation and prediction by Cimmino [3], Lee [4], and Sterpu [5] in various contexts.

In the military context, Surma [6] presents a comprehensive review of how recent advances in Deep Learning are driving innovation in military domains, particularly enhancing intelligence operations and autonomous platforms. Also, Baeza [7] provided an overview of emerging trends in defense communications. Likewise, Hao [8] and Wang [9] focused on predicting flight trajectories of aircraft. However, there remains unexplored potential in artillery applications.

A persistent challenge in external ballistics is accurately modeling aerodynamic forces on large projectiles such as 155 mm shells. Traditionally, these forces are estimated using analytical models and aerodynamic coefficients derived from experiments or computational tools like PRODAS [10]. Computational Fluid Dynamics (CFD) has also been employed for determining these coefficients, as demonstrated by Silva [11]. While effective, such classical models can lack flexibility and often require significant computational effort when simulating varying firing conditions.

This study goes a step further and tries to implement a hybrid approach that integrates analytical models with neural networks to estimate aerodynamic forces on artillery shells based on their aerodynamic coefficients during their trajectory. A machine learning model was trained using data generated by PRODAS, encompassing a range of firing conditions including elevation angle, velocity, and atmospheric parameters. The neural network estimates key forces acting on the projectile—lift, drag, Magnus force, damping forces, and angular restoring

moment. Model performance was rigorously evaluated through: (i) direct comparison with the PRODAS dataset; (ii) implementation in a four degrees-of-freedom (4-DOF) ballistic simulation adhering to NATO standards STANAG 4355 [12], 4119 [13], and 4044 [14]; and (iii) trajectory comparisons against data from three live firing tests and the corresponding firing tables.

The objective of this hybrid method is to assess potential benefits in adaptability and possible applications, with an eye toward future onboard real-time computation, dynamic correction of fire parameters, and integration into autonomous fire control systems. By bridging analytical and data-driven techniques, the approach aims to provide a accurate alternative to classical ballistic models.

2 Ballistic Model

2.1 Equation of Motion

The ballistic model used in this study follows a modified point-mass formulation compliant with NATO STANAG 4355 incorporating the main forces acting on the projectile in free flight. In the eq. (1) the motion of the projectile's center of gravity (CG) is governed by the combined effects of drag (**DF**), lift (**LF**), Magnus (**MF**), and gravity (**P**). The model also includes Coriolis acceleration λ, relevant for long-range trajectories, with m as the mas of the grenade.

$$\sum \boldsymbol{F} = m\dot{\boldsymbol{u}} = \boldsymbol{DF} + \boldsymbol{LF} + \boldsymbol{MF} + \boldsymbol{P} + m\boldsymbol{\lambda} \tag{1}$$

From the aerodynamic forces, the CG acceleration is obtained, allowing the projectile's velocity **u(t)** to be determined by integration as seen in the eq. (2), using the muzzle exit velocity $\boldsymbol{u_0}$ in the direction of the gun line as the initial condition. Subsequently, the position **X(t)** is computed by integrating the velocity over time as seen in the eq. (3), with the origin defined as the starting point of the trajectory.

$$\boldsymbol{u}(t) = \boldsymbol{u_0} + \int_0^t \dot{\boldsymbol{u}}\, dt \tag{2}$$

$$\boldsymbol{X}(t) = \int_0^t \boldsymbol{u}\ \ dt \tag{3}$$

The aerodynamic forces are applied at the projectile's center of pressure (CP) and are highly dependent on the relative velocity between the projectile and the atmospheric flow. In the eq. (4), the wind velocity relative to the ground is denoted by **W**, the relative airspeed **v** is defined as the difference **u – W**. In th eq. (5) the angle between the relative velocity vector *v* and the projectile's longitudinal axis χ is defined as the angle of attack α, a variable of critical importance for determining the aerodynamic forces.

$$\boldsymbol{v} = \boldsymbol{u} - \boldsymbol{W} \tag{4}$$

$$\alpha = acos\left(\frac{\boldsymbol{v}\cdot\boldsymbol{X}}{\boldsymbol{v}}\right) \tag{5}$$

In addition to forces, the projectile experiences aerodynamic moments at its CG, causing undesired pitching motion that affects stability and efficiency. To counter this, rifled barrels impart a stabilizing spin along the longitudinal axis, leveraging angular momentum conservation.

Equations (6), (7), and (8) define the angular velocity components ω, initially set by the ratio between muzzle velocity $\boldsymbol{u_0}$ and rifling twist rate tc. During flight, aerodynamic effects alter both the orientation $\boldsymbol{\chi}$ and ω itself. Considering local air density ρ and damping coefficients, ω evolves over time according to differential equations involving parameters like the spin damping moment coefficient Cspin.

$$\omega_{x0} = \frac{2\pi |\boldsymbol{u_0}|}{t_c d} \tag{6}$$

$$\dot{\omega}_x = \frac{\pi \ \rho \ d^4 \ \omega_x \ C_{spin}}{8 \ I_x} \tag{7}$$

$$\omega_x = \omega_{x0} + \int_0^t \dot{\omega}_x dt \tag{8}$$

The model includes spin-induced yaw $\boldsymbol{\alpha_R}$, a secondary effect influenced by gravity and stabilizing spin, determined by the eq. (9). In flight, $\boldsymbol{\alpha_R}$ tends toward an equilibrium angle, determined by the angle of attack α and moment coefficients $C_{(M\alpha)}$ and $C_{(M\alpha^3)}$. Initially zero, it evolves due to the projectile–fluid interaction.

$$\boldsymbol{\alpha_R} = \frac{8 I_x \omega_x \boldsymbol{v} \times \dot{\boldsymbol{u}}}{\pi \rho d^3 (C_{(M\alpha)} + C_{(M\alpha^3)} |\boldsymbol{\alpha_R^2}|) \boldsymbol{v}^4} \tag{9}$$

2.2 Aerodynamic Forces

The gravitational acceleration acting on the projectile is calculated by considering the latitude of the trajectory's origin. The gravity **g**, in the eq. (10), it is expressed as a function of the reference gravity magnitude g_0, which is adjusted according to the latitude (lat) as seen in the eq. (11). The position of the projectile's center of mass relative to the center of the Earth is represented by the vector **r** in the eq. (12) while the Earth's radius at the origin point is assumed to be constant R, with an approximate value of 6,356,766 meters.

$$\boldsymbol{g} = -g_0 \left(\frac{R^2}{r^3} \cdot \boldsymbol{r}\right) \tag{10}$$

$$g_0 = 9{,}80655 \left(1 - 0{,}0026 \left(2 \cdot lat\right)\right) \tag{11}$$

$$\boldsymbol{r} = \boldsymbol{X} + \begin{bmatrix} 0 & 0 & R \end{bmatrix} \tag{12}$$

The acceleration resulting from the Coriolis effect in the eq. (13) is determined based on the Earth's rotation vector **Ω**, whose magnitude is 7.292115×10^{-5} rad/s. This effect depends on the orientation of the trajectory relative to geographic north and is influenced by the azimuth (AZ), which can be seen in the eq. (14).

$$\boldsymbol{\lambda} = -2 \left(\boldsymbol{\Omega} \times \boldsymbol{u}\right) \tag{13}$$

$$\boldsymbol{\Omega} = \begin{bmatrix} \Omega \cos\left(lat\right) \cos\left(AZ\right) \\ \Omega \cos\left(lat\right) sen\left(AZ\right) \\ \Omega \, sen\left(lat\right) \end{bmatrix} \tag{14}$$

In the eq. 15, the drag force **DF**, acting along **v**, is defined using the form factor i, drag coefficients C_{d0}, $C_{(d\alpha^2)}$, $C_{(d\alpha^4)}$, and yaw factor Q_d. Here, i and Q_d are set to 1, and only up to the quadratic term is used.

$$\boldsymbol{DF} = -\left(\frac{\pi \rho d^2 i |\boldsymbol{v}|}{8}\right) \left[C_{d0} + C_{(d\alpha^2)} \left(Q_d \alpha_R\right)^2 + C_{(d\alpha^4)} \left(Q_d \alpha_R\right)^4\right] \cdot \boldsymbol{v} \tag{15}$$

In the eq. 16, the lift force **LF**, acting orthogonal to the relative velocity **v**, is modeled by a polynomial in the lift yaw angle $\boldsymbol{\alpha_R}$, using coefficients C_{L0}, $C_{(L\alpha^3)}$, $C_{(L\alpha^5)}$, and the lift factor fL. In this study, fL=1, and terms beyond the cubic coefficient are neglected.

$$\boldsymbol{LF} = -\left(\frac{\pi f L \rho d^2 v^2}{8}\right)\left[C_{L0} + C_{(L\alpha^3)}(\alpha_R)^3 + C_{(L\alpha^5)}(\alpha_R)^5\right]\cdot\boldsymbol{\alpha_R} \tag{16}$$

In the eq. 17, the Magnus force **MF** depends on the lift yaw angle $\boldsymbol{\alpha_R}$, and includes the correction factor Q_M, and the Magnus coefficient Cmag, which adjust the force magnitude based on projectile features and flight conditions. In this work Q_M is considered equal to 1.

$$\boldsymbol{MF} = -\left(\frac{\pi \rho d^3 \omega_x Q_M C_{mag}}{8}\right)\left(\boldsymbol{\alpha_R} \times \mathbf{v}\right) \tag{17}$$

3 Methodology

3.1 Neural Network Architecture

The architecture is a fully connected feedforward neural network with two hidden layers of eight neurons each. This topology was defined empirically through iterative testing to balance computational cost and generalization. Sigmoid activation functions (eq. 18) were used in the hidden layers, while the output layer remained linear to preserve the physical scale of the results, where *y* represents the output from the previous layer. The network was trained via supervised learning using the Adam optimizer, a fixed learning rate of 1×10^{-4}, and full-batch gradient descent.

$$\sigma(y) = \frac{1}{1+\exp(-y)} \tag{18}$$

The inputs are the Mach number and the magnitude of the angle of attack $\boldsymbol{\alpha_R}$, sampled uniformly over ranges typical for artillery firings, with $\boldsymbol{\alpha_R}$ varying from 0 to 0.3 radians. The network outputs correspond to five aerodynamic components used in the 4-DOF ballistic model: drag, lift, Magnus force, roll damping, and the moment associated with the angle of repose. Inputs were normalized to the [0, 1] range, while outputs remained unnormalized to preserve their physical interpretation.

Training was conducted for 100,000 epochs, minimizing mean squared error (MSE) calculated as the average residual across the dataset. No regularization or early stopping was used, since the dataset was controlled and the objective was to assess network fidelity across a complete and uniform sample space.

3.2 Projectile Firing and Analysis Using the Modified Point-Mass Model

To validate the neural network's performance, seven real 155 mm firings were analyzed under atmospheric conditions near the International Standard Atmosphere (ISA). Each shot had an ambient temperature around 15 °C, air density of 1.225 kg/m³, latitude near zero, and azimuth toward geographic north. Wind data were obtained from meteorological reports at firing times. Gun drift was measured as the angular difference between the line of fire and the plane defined by the gun and impact point. The conditions of fire are displayed in Table 1.

Table 1. Artillery firing Conditions

Shot	Elevation (rad)	Drift (rad)	Crosswind (m/s)	Headwind (m/s)	Range (m)
1st	0.1102	0.00398	0.51	1.03	5
2nd	0.2349	0.00776	~0.00	1.54	8

3rd	0.3431	0.0116	0.51	1.54	10
4th	0.4295	0.0166	1.03	1.03	12
5th	1.0899	0.0748	1.03	-0.51	12
6th	1.1920	0.1134	~0.00	1.03	10

Elevation angles were set using firing tables to ensure desired ranges under specific atmospheric conditions. The propellant charge yielded a muzzle velocity of 565.4 m/s. Each case was simulated with both the traditional analytical aerodynamic model and the modified version incorporating neural network estimates.

4 Results and Discussion

The analysis of the neural network training results showed stable and efficient convergence. Figure 1 displays the loss function (mean squared error, MSE) evolution on a logarithmic scale. A sharp decrease occurred early in training, with the error dropping from about 10^{-1} to near 10^{-2} before the 10,000 epochs. Thereafter, learning slowed asymptotically, reaching approximately 3.2×10^{-3} in the 100,000 epoch.

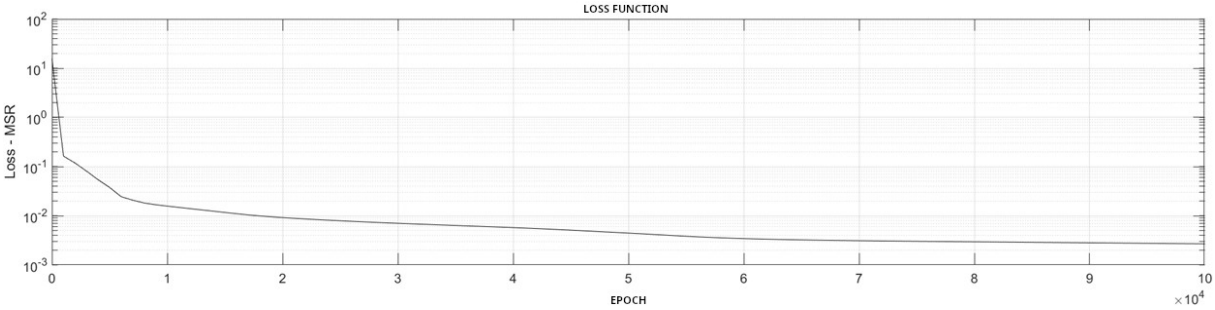


Figure 1: Evolution of the Loss Function During Training

The network's predictive ability was assessed using the coefficient of determination (R^2) for each of the five aerodynamic components, calculated over the training dataset. High correlations were achieved: drag force ($R^2 = 0.9355$), lift force ($R^2 = 0.9940$), spin damping ($R^2 = 0.9984$), overturning moment ($R^2 = 0.9983$), and Magnus force ($R^2 = 0.9056$), with the latter showing slightly lower accuracy.

To validate the model's performance, trajectory simulations incorporating the neural network were compared against real artillery shots. As shown in Table 2, the results support the network's capacity to replicate aerodynamic behavior with sufficient fidelity to complement or partially replace traditional formulations in ballistic modeling.

Table 2. Artillery firing simulation results

Shot	Model	Estimated Range (m)	Range Error (%)	Drift (m)
1st	Conventional	5109,2	2,18	3,6
	Neural Network	5042,2	0,84	3,6
2nd	Conventional	8374,3	4,68	14
	Neural Network	8287	3,59	14
3rd	Conventional	10482	4,82	25
	Neural Network	10412	4,12	25
4th	Conventional	12301	2,51	44
	Neural Network	12224	1,87	46
5th	Conventional	12324	2,7	298
	Neural Network	12132	1,1	289
6th	Conventional	10303	3,03	476
	Neural Network	10153	1,53	462

Comparatively, both methods approximate trajectories reasonably, though the neural network consistently lowers range and lateral deviation, yielding slightly better overall impact predictions. This may reflect the network's tendency to smooth aerodynamic coefficients, which can result in better precision. The only exception was fourth shot, with a Drift higher than the conventional model, however, if we consider the total distance from the impact point, the conventional model represents a difference of 304,2 meters and the hybrid models sits at 228,67 m, which is still a better prediction.

Furthermore, Figure 2 compares the sixth shot's simulated trajectories from the conventional model (blue thick line) and neural network (red thin line). Both show similar ascent and agree closely to the apogee, but diverge progressively during descent, indicating significant neural network differences affecting the final of the trajectory.

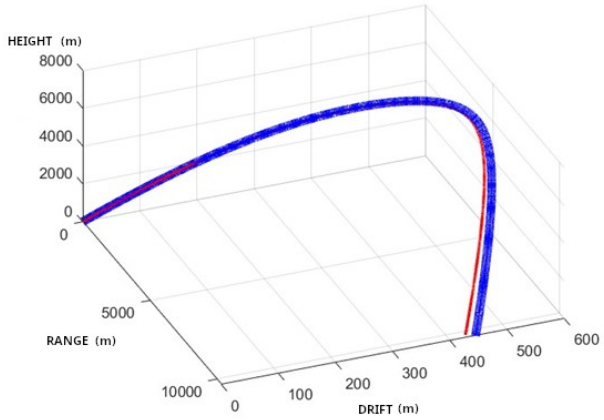


Figure 2: Comparison of Simulated Flight Trajectories

5 Conclusions

This study proposed and validated a hybrid methodology that integrates traditional analytical formulations with neural networks to estimate aerodynamic forces on 155 mm artillery projectiles. Using the PRODAS dataset and real artillery data (including variations in elevation angle, gun drift, and wind) the neural network achieved high predictive accuracy, with correlation coefficients above 0.99 for most aerodynamic components. Embedded in a 4-DOF ballistic simulator compliant with NATO STANAGs 4355, 4119, and 4044, the hybrid model outperformed the conventional methods, reducing the overall error across six scenarios.

Even when drift values were similar, the hybrid model produced smaller overall impact errors, highlighting its capacity to capture complex aerodynamic effects. In addition to improved precision, the method retains the consistency and interoperability of classical physics-based models. These features support its potential use in real-time fire control, onboard systems, and applications with direct neural network integration in trajectory prediction, advancing beyond existing studies.

The framework also lays groundwork for future extensions, such as adapting the model for full 6-DOF simulations, enriching the training set with firing tables, or exploring predictive use in complex missions like intercepting aerial or mobile targets. This work represents a relevant step toward smarter artillery systems and advanced decision-support tools.

Acknowledgements. The author acknowledges the *Diretoria de Fabricação do Exército Brasileiro* for the institutional support provided during the development of this research.

Authorship statement. The authors hereby confirm that they are the sole liable persons responsible for the authorship of this work, and that all material that has been herein included as part of the present paper is either the property (and authorship) of the authors, or has the permission of the owners to be included here.

References

[1] P. M. Kebria, A. Khosravi, S. M. Salaken and S. Nahavandi, "Deep imitation learning for autonomous vehicles based on convolutional neural networks," in *IEEE/CAA Journal of Automatica Sinica*, vol. 7, no. 1, pp. 82-95, January 2020, doi: 10.1109/JAS.2019.1911825.

[2] Waseem Ullah, Amin Ullah, Tanveer Hussain, Khan Muhammad, Ali Asghar Heidari, Javier Del Ser, Sung Wook Baik, Victor Hugo C. De Albuquerque, Artificial Intelligence of Things-assisted two-stream neural network for anomaly detection in surveillance Big Video Data, Future Generation Computer Systems, Volume 129, 2022, Pages 286-297, ISSN 0167-739X, https://doi.org/10.1016/j.future.2021.10.033.

[3] N. Cimmino, D. Amato, R. Opromolla, G. Fasano, A recurrent neural network-based approach for ballistic coefficient estimation of resident space objects in low earth orbit, Advances in Space Research, Volume 75, Issue 2, 2025, Pages 2088-2107, ISSN 0273-1177, https://doi.org/10.1016/j.asr.2024.11.055.

[4] LEE, Dong Ho; LEE, DongUk; HAN, Seoeum; SEO, Seongil; LEE, Bok Jik; AHN, Jaemyung. *Deep residual neural network for predicting aerodynamic coefficient changes with ablation*. Aerospace Science and Technology, v. 136, art. 108207, maio 2023. Disponível em: https://doi.org/10.1016/j.ast.2023.108207. Acesso em: 25 jul. 2025.

[5] STERPU, Diana-Andreea; MĂRIUȚA, Daniel; CICAN, Grigore; LARCO, Ciprian-Marius; GRIGORIE, Lucian-Teodor. *Machine Learning Prediction of Airfoil Aerodynamic Performance Using Neural Network Ensembles*. Applied Sciences, v. 15, n. 14, art. 7720, 2025. Disponível em: https://doi.org/10.3390/app15147720. Acesso em: 25 jul. 2025.

[6] SURMA, Jerzy. *Deep Learning in Military Applications: Threats and Opportunities*. Safety & Defense, v. 10, n. 1, p. 1–10, 2024. DOI: https://doi.org/10.37105/sd.214.

[7] BAEZA, Victor Monzon; PARADA, Raúl; SALOR, Laura Concha; MONZO, Carlos. *AI-Driven Tactical Communications and Networking for Defense: A Survey and Emerging Trends*. arXiv:2504.05071 [eess.SY], 2025. Disponível em: https://doi.org/10.48550/arXiv.2504.05071. Acesso em: 25 jul. 2025.

[8] HAO, Qinzhi; ZHANG, Jiali; JING, Tengyu; WANG, Wei. *Flight trajectory prediction using an enhanced CNN-LSTM network*. arXiv:2404.19218 [cs.LG], 2024. Disponível em: https://doi.org/10.48550/arXiv.2404.19218. Acesso em: 25 jul. 2025.

[9] Wang, X. et al. (2023). TraNet: A Hybrid Deep Neural Network for Long-Time-Scale Aircraft Trajectory Prediction. In: Yan, L., Duan, H., Deng, Y. (eds) Advances in Guidance, Navigation and Control. ICGNC 2022. Lecture Notes in Electrical Engineering, vol 845. Springer, Singapore. https://doi.org/10.1007/978-981-19-6613-2_429

[10] ARROW TECH. Projectile Rocket Ordnance Design & Analysis System- PRODAS.

[11] SILVA, Wallace Ramos Rosendo ; Rezende, A. L. T. . Study of ballistic parameters for projectile range extension. In: CILAMCE 2022 - XLIII Ibero-Latin American Congress on Computational Methods in Engineering, 2022, Foz do Iguaçu - PR. Proceedings of the Ibero-Latin-American Congress on Computational Methods in Engineering, 2022. p. 2675-6269.

[12] NATO STANDARTIZATION AGENCY. STANAG 4355- The Modified Point Mass And Five Degrees Of Freedom Trajectory Models. 3. ed. Bruxelas, Bélgica: NATO Standar tization Agency, 2009.

[13] NATO STANDARTIZATION AGENCY. STANAG 4119-Adoption Of A Standart Cannon Artillery Firing Table Format. 2. ed. Bruxelas, Bélgica: NATO Standartization Agency, 2007.

[14] NATO STANDARTIZATION AGENCY. STANAG 4044- Adoption Of A Standard Atmosphere. 2. ed. Bruxelas, Bélgica: Military Agency for Standartization (MAS), 1969.